# Supporting Information for "Observed equatorward propagation and chimney effect of near-inertial waves in the mid-latitude ocean"

Xiaolong Yu[1,2,3], Alberto C. Naveira Garabato[4], Clément Vic[5], Jonathan Gula[5,6], Anna C. Savage[7], Jinbo Wang[8], Amy F. Waterhouse[7], Jennifer A. MacKinnon[7]

[1]School of Marine Sciences, Sun Yat-sen University, Zhuhai, China

[2]Southern Marine Science and Engineering Guangdong Laboratory (Zhuhai), Zhuhai, China

[3]Guangdong Provincial Key Laboratory of Marine Resources and Coastal Engineering, Guangzhou, China

[4]Ocean and Earth Science, University of Southampton, Southampton, UK

[5]Univ Brest, CNRS, IRD, Ifremer, Laboratoire d'Océanographie Physique et Spatiale (LOPS), IUEM, Brest, France

[6]Institut Universitaire de France (IUF), Paris, France

[7]Scripps Institution of Oceanography, University of California, San Diego, La Jolla, California, USA

[8]Jet Propulsion Laboratory, California Institute of Technology, Pasadena, California, USA

## Contents of this file

## Text S1. Wentzel-Kramers-Brillouin scaling

The amplitude and wavenumber of NIWs change with the varying vertical stratification in the ocean due to refraction (Leaman & Sanford, 1975). To account for this effect, 'Wentzel-Kramers-Brillouin (WKB) scale' and 'WKB stretch' are typically applied (e.g., Bell, 1974; Duda & Cox, 1989). As previous OSMOSIS studies have shown that the region underwent a seasonal cycle on the vertical stratification (e.g., Buckingham et al., 2016; Erickson et al., 2020), monthly moving averaged buoyancy frequency is used to get WKB scaling from the time series of horizontal velocity. The WKB-scaled (denoted by the superscript '$WKB$') near-inertial kinetic energy is computed as

$$KE_{NI}^{WKB} = \frac{\overline{N}(t)}{N(t,z)} KE_{NI}, \tag{1}$$

where $t$ is the time, $z$ is the vertical coordinate, $N = \sqrt{-(g/\rho_0)(\partial\rho/\partial z)}$ is the buoyancy frequency with $g$ as gravity and $\rho$ as potential density, and $\overline{N}$ denotes the depth-mean buoyancy frequency between 50 and 520 m. Similarly, the WKB-scaled near-inertial vertical shear is computed as

$$S_{NI}^{WKB} = \frac{\overline{N}(t)}{N(t,z)} |\partial \boldsymbol{u}_{NI}/\partial z|^2. \tag{2}$$

To account for vertical wavenumber changes, the WKB-stretched depth is computed as

$$z^{WKB} = \int_{-50}^{z} \frac{N(z)}{\overline{N}}\, dz, \tag{3}$$

where $z^{WKB}$ is the stretched vertical coordinate. Quantitative calculations such as the seasonal rotary vertical wavenumber spectrum are computed in the stretched coordinates (Figure S3).

**Text S2. Slab model**

Slab models have been found appropriate for reproducing near-inertial motions in the mixed layer from time series of wind alone (e.g., Pollard & Millard, 1970; Plueddemann & Farrar, 2006). The corresponding momentum equation can be expressed as

$$\frac{d\widetilde{\boldsymbol{u}}}{dt} + (r + if)\widetilde{\boldsymbol{u}} = \frac{\widetilde{\boldsymbol{\tau}}}{\rho_0 H_{ML}}, \tag{4}$$

where $\widetilde{(.)}$ denotes the complex format (e.g., $\widetilde{\mathbf{u}} = u + iv$), $r$ is a damping constant that parameterizes the transfer of energy from the mixed layer to the ocean interior and $H_{ML}$ is the mixed layer depth. Here we use a damping factor $r = 0.04f$ ($r^{-1} \sim 16.7$ days), consistent with previous work (e.g., D'Asaro, 1985; Alford et al., 2012). The 10-day smoothed mixed layer depth estimated from the OSMOSIS gliders is used. The slab model is solved using the traditional time-stepping method (D'Asaro, 1985).

**Text S3. Dispersion relation and near-inertial properties**

Following Gill (1982), the dispersion relation for NIWs in the absence of background flows is given by

$$(\omega^2 - f^2)m^2 = N^2 k_h^2, \tag{5}$$

where $\omega$ is the frequency, $m$ the vertical wavenumber and $k_h$ the horizontal wavenumber. The vertical group speed $c_{gz}$ can then be derived by taking the derivative of the dispersion relation with respect to vertical wavenumber, yielding

$$c_{gz} = \frac{\partial \omega}{\partial m} = (\omega^2 - f^2)/\omega m. \tag{6}$$

Similarly, the horizontal group speed $c_{gh}$ can be estimated by

$$c_{gh} = \frac{\partial \omega}{\partial k_h} = N\sqrt{\omega^2 - f^2}/\omega m. \tag{7}$$

Thus, a relationship between $c_{gz}$ and $c_{gh}$ can be obtained as follows:

$$\frac{c_{gz}}{c_{gh}} = \sqrt{\omega^2 - f^2}/N. \tag{8}$$

From equation (8) and mooring-inferred horizontal and vertical group speeds, the equation for $\omega$ is

$$\omega = \sqrt{f^2 + N^2 \frac{(c_{gz}^{obs})^2}{(c_{gh}^{obs})^2}}. \tag{9}$$

Then the horizontal wavenumber can be obtained by

$$k_h = \sqrt{\frac{(\omega^2 - f^2)m^2}{N^2}}. \tag{10}$$

The buoyancy frequency $N = 3.5 \times 10^{-3}$ rad s$^{-1}$ ($N/f \sim 31$) is computed from climatological temperature and salinity profiles of the World Ocean Atlas 2018 (Garcia et al., 2019), and then averaged over the 50−520-m depth range.

## References

Alford, M. H., Cronin, M. F., & Klymak, J. M. (2012). Annual cycle and depth penetration of wind-generated near-inertial internal waves at ocean station papa in the northeast pacific. *Journal of Physical Oceanography*, *42*(6), 889-909.

Bell, T. H. (1974). Processing vertical internal wave spectra. *Journal of Physical Oceanography*, *4*, 669–670.

Buckingham, C. E., Garabato, A. C. N., Thompson, A. F., Brannigan, L., Lazar, A., Marshall, D. P., ... Belcher, S. E. (2016). Seasonality of submesoscale flows in the ocean surface boundary layer. *Geophysical Research Letters*, *43*(5), 2118-2126.

D'Asaro, E. A. (1985). The energy flux from the wind to near-inertial motions in the surface mixed layer. *Journal of Physical Oceanography*, *15*(8), 1043-1059.

Duda, T. F., & Cox, C. S. (1989). Vertical wave number spectra of velocity and shear at small internal wave scales. *Journal of Geophysical Research*, *94*(C1), 939.

Erickson, Z. K., Thompson, A. F., Callies, J., Yu, X. L., Garabato, A. N., & Klein, P. (2020). The vertical structure of open-ocean submesoscale variability during a full seasonal cycle. *Journal of Physical Oceanography*, *50*(1), 145-160.

Garcia, H. E., Boyer, T. P., Baranova, O. K., Locarnini, R. A., Mishonov, A. V., Grodsky, A., ... Zweng, M. M. (2019). *World Ocean Atlas 2018: Product documentation* (A. Mishonov, Ed.).

Gill, A. E. (1982). *Atmosphere-ocean dynamics*. Academic Press New York.

Leaman, K. D., & Sanford, T. B. (1975). Vertical energy propagation of inertial waves - vector spectral analysis of velocity profiles. *Journal of Geophysical Research*, *80*(15), 1975-1978.

Plueddemann, A. J., & Farrar, J. T. (2006). Observations and models of the energy flux from the wind to mixed-layer inertial currents. *Deep-Sea Research Part II-Topical Studies in Oceanography*, *53*(1-2), 5-30.

Pollard, R. T., & Millard, R. C. (1970). Comparison between observed and simulated wind-generated inertial oscillations. *Deep-Sea Research*, *17*(4), 813-821.

**Table S1.** Detailed properties of the six near-inertial events derived from the mooring observations combined with the dispersion relation.

| Event | $c_{gz}^{obs}$ [m d$^{-1}$] | $c_{gh}^{obs}$ [m day$^{-1}$] | $\omega$ | $2\pi/m$ [m] | $2\pi/k_h$ [km] |
|---|---|---|---|---|---|
| 1 | 79 | 5875 | $1.065f$ | 781 | 69 |
| 2 | 59 | 6653 | $1.036f$ | 787 | 94 |
| 3 | 50 | 5270 | $1.026f$ | 342 | 48 |
| 4 | 75 | 4838 | $1.058f$ | 513 | 48 |
| 5 | 47 | 7085 | $1.023f$ | 791 | 119 |
| 6 | 58 | 5270 | $1.029f$ | 698 | 93 |
| mean±std | 61±13 | 5875±864 | $1.039\pm0.018f$ | 652±185 | 79±28 |

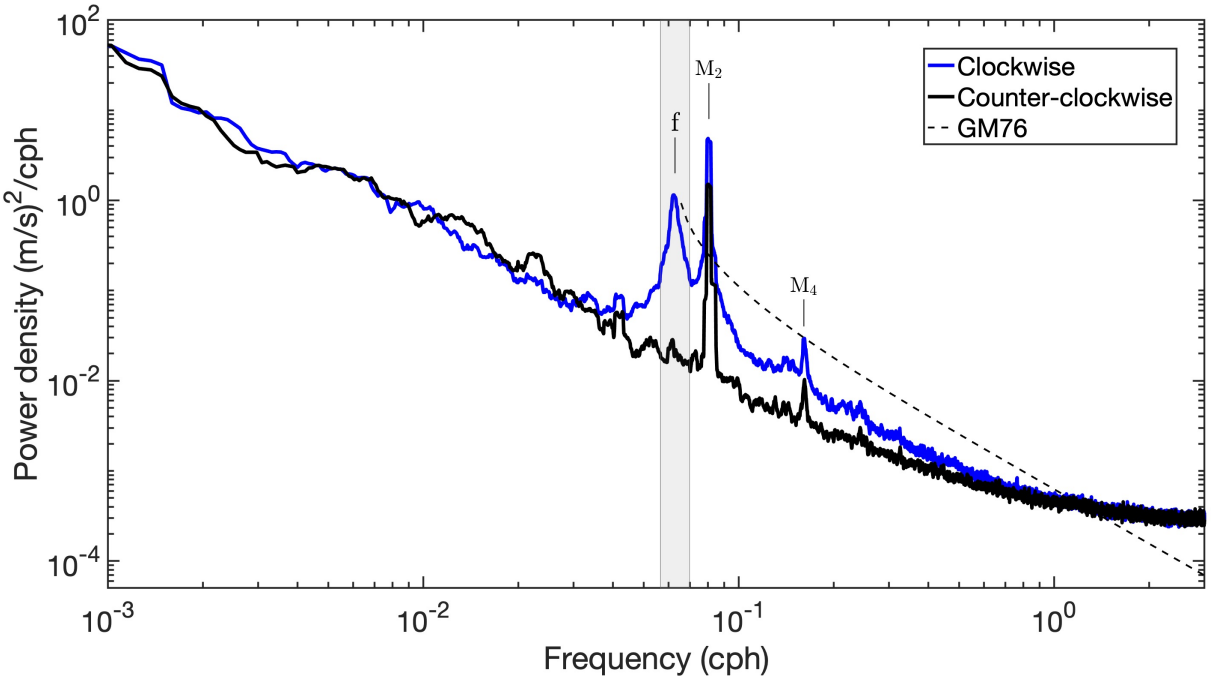


**Figure S1.** Rotary frequency spectrum of WKB-scaled horizontal velocity measured by the top current meter on the central mooring with the record period September 2012 – September 2013. The clockwise and counter-clockwise components of the spectrum are blue and black, respectively. The GM76 model spectrum is indicated by a black dashed curve. The inertial peak (1/15.91 cph), M2 (1/12.42 cph) and M4 (1/6.21 cph) tidal peaks are marked. The light grey shaded region indicates the near-inertial band used in band-pass filter to isolate near-inertial signals.

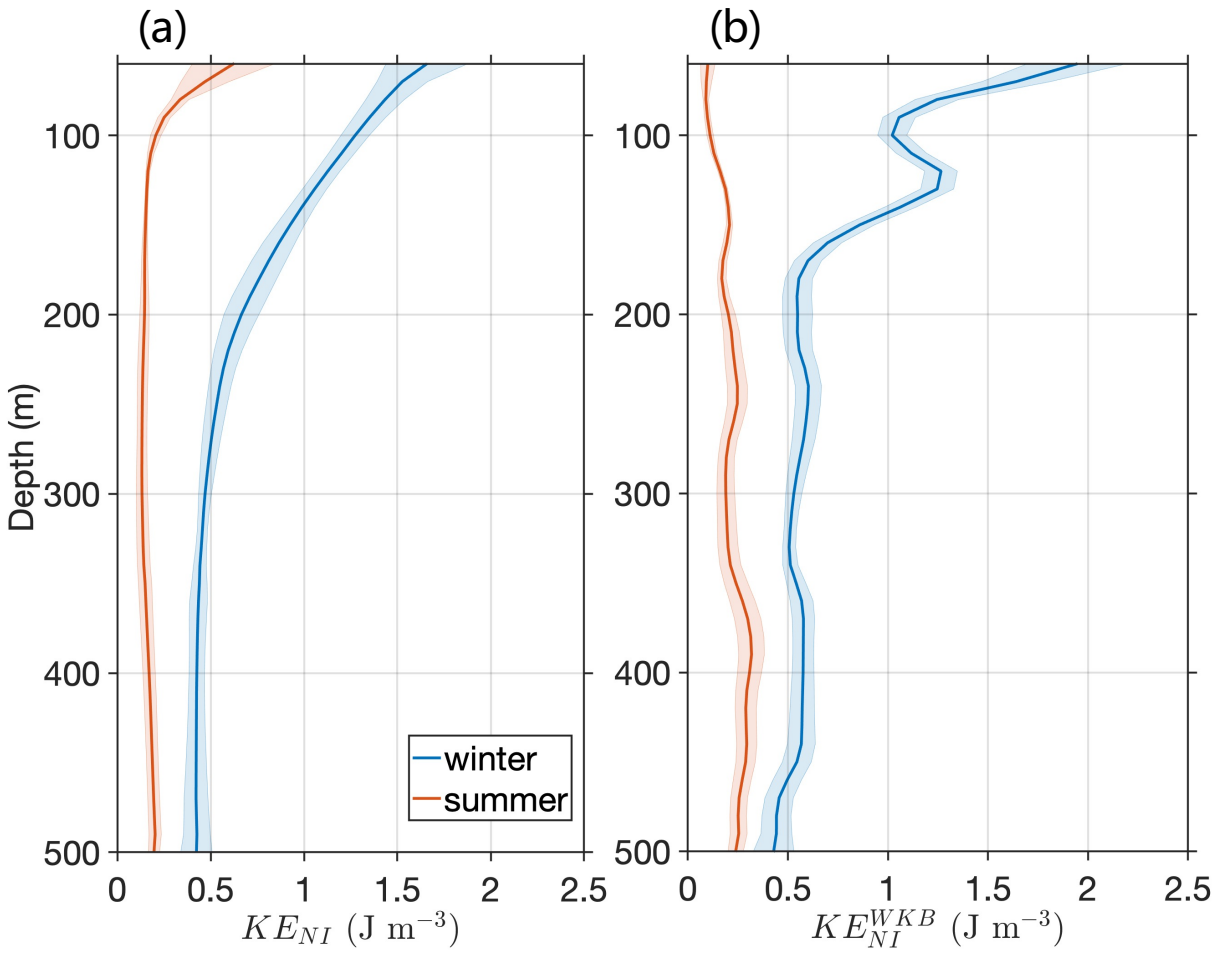


**Figure S2.** The time-mean profiles (solid lines) and one standard deviation envelope respective to all nine moorings (shading) of (a) measured and (b) WKB-scaled near-inertial kinetic energy in winter (December-February; blue) and summer (June-August; orange).

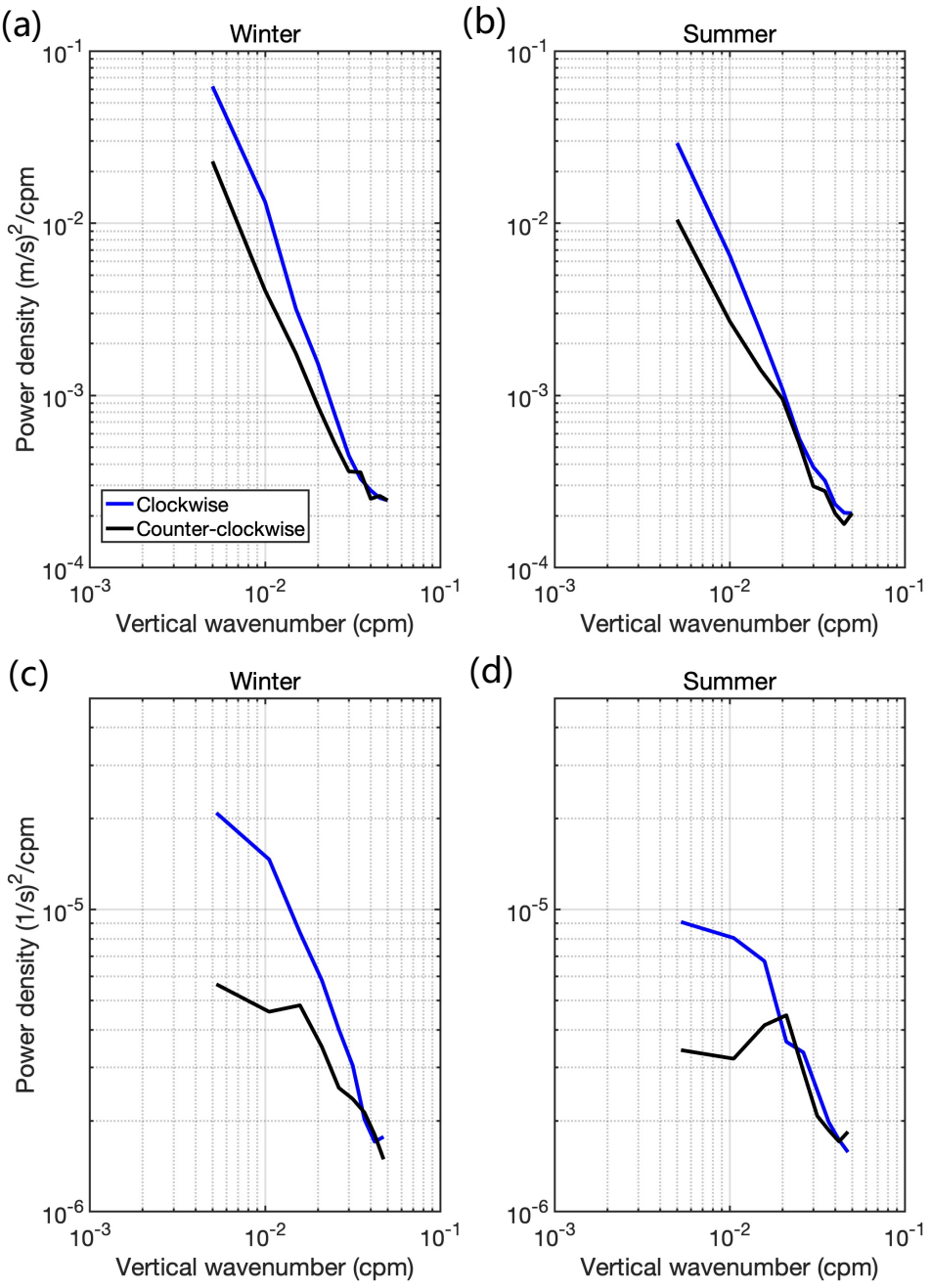


**Figure S3.** Rotary vertical wavenumber spectra of the WKB-scaled near-inertial velocity profiles (top) and the WKB-scaled near-inertial vertical shear profiles (bottom) from the ADCP measurements, showing the clockwise (blue) and the counter-clockwise (black) components. The (left) wintertime and (right) summertime horizontal velocity spectra are calculated as the mean of respective period.

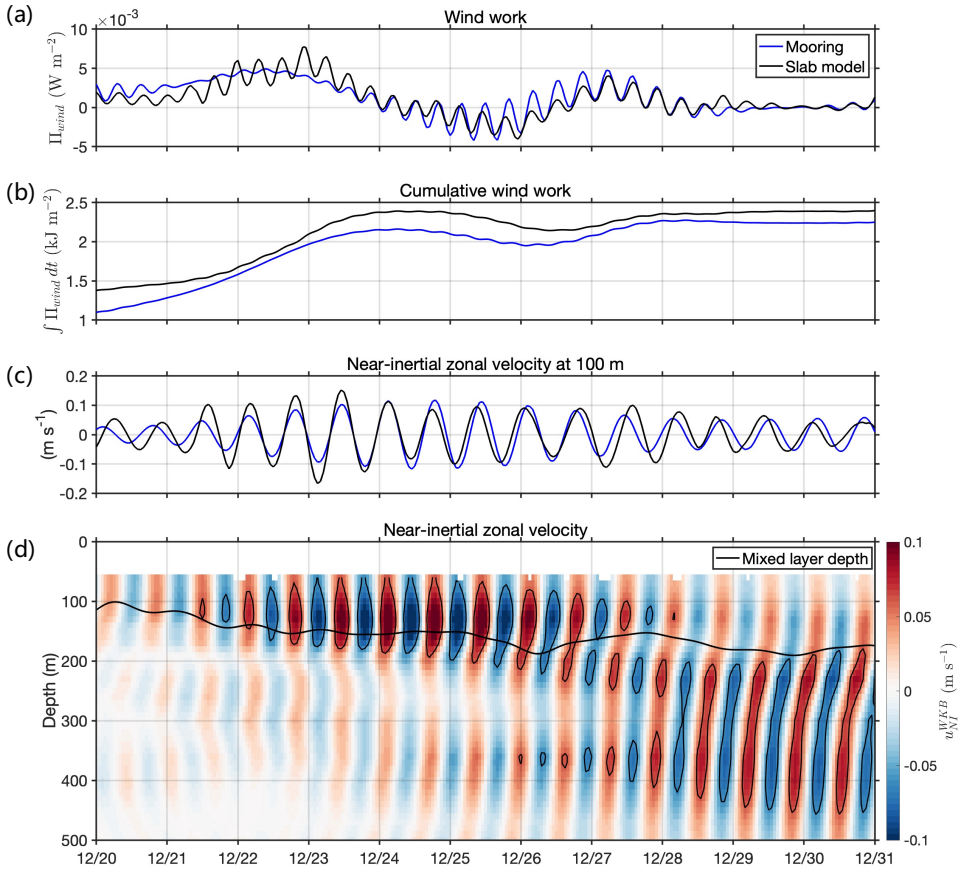


**Figure S4.** Observed and modeled wind work and upper-ocean currents during a near-inertial wave event (20 - 31 December 2012). (a) Energy flux into near-inertial motions from observed mixed-layer near-inertial currents and reanalysis winds (blue line) and slab model driven by reanalysis winds (black line). (b) The time integral of (a) showing the cumulative energy input to the mixed layer from each flux estimate. (c) Zonal mixed-layer near-inertial current from the top ACM sensor (blue), and zonal mixed-layer current estimated from the slab model driven by reanalysis winds (black). (d) Near-inertial zonal velocity from the ACMs. Black contours mark the velocity of 0.1 m $s^{-1}$. The black line represents the glider-derived mixed layer depth.

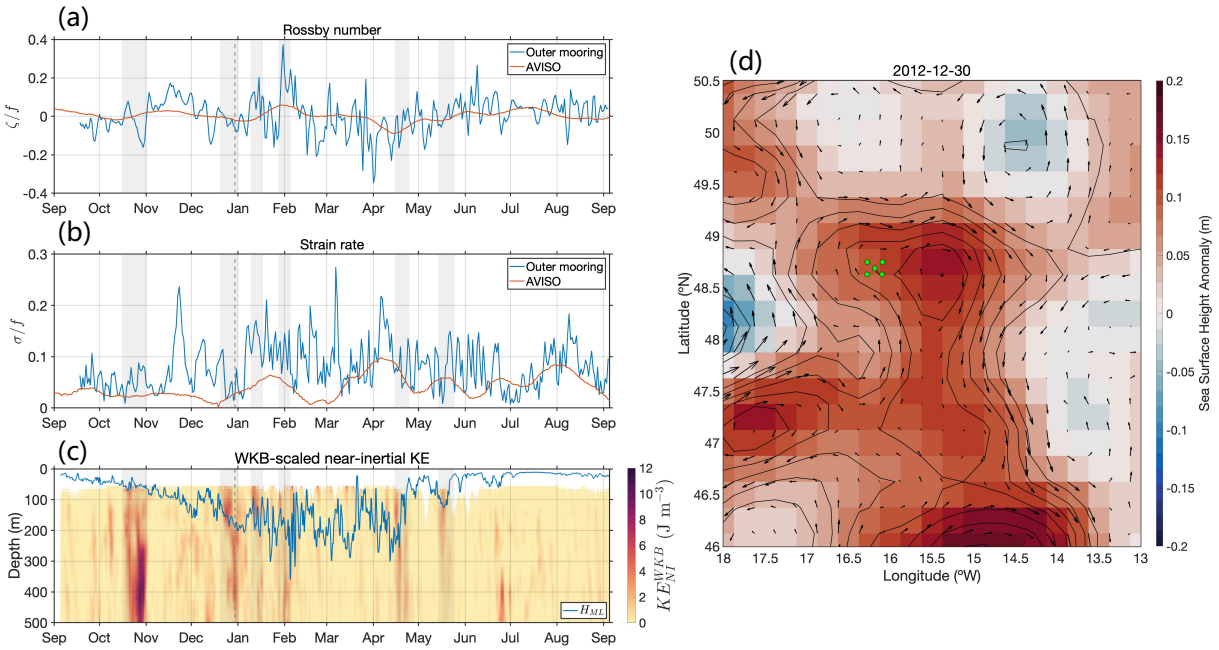


**Figure S5.** (a) Time series of Rossby number estimated from the outer moorings (depth-averaged; blue) and altimetric measurements (orange). (b) Time series of strain rate estimated from the outer moorings (depth-averaged; blue) and altimetric measurements (orange). (c) WKB-scaled near-inertial kinetic energy observed from the current meters at the central mooring. The blue line indicates the glider-based mixed layer depth $H_{ML}$. Grey shaded regions in (a-c) indicate the six wind-generated events of NIWs. (d) Snapshot of sea level anomaly on 30 December 2012 with surface geostrophic current velocity shown as black vectors and the sea level anomaly contours (0.04-m interval, ranging from -0.2 to 0.2 m). Sea level anomaly and surface geostrophic velocity data are obtained from the delayed-time gridded 0.25°×0.25° AVISO (Archiving, Validation and Interpretation of Satellite Oceanographic Data) product. The green dots indicate the location of the OSMOSIS central and outer moorings. The grey dashed lines in (a-c) indicate the time of 30 December 2012.

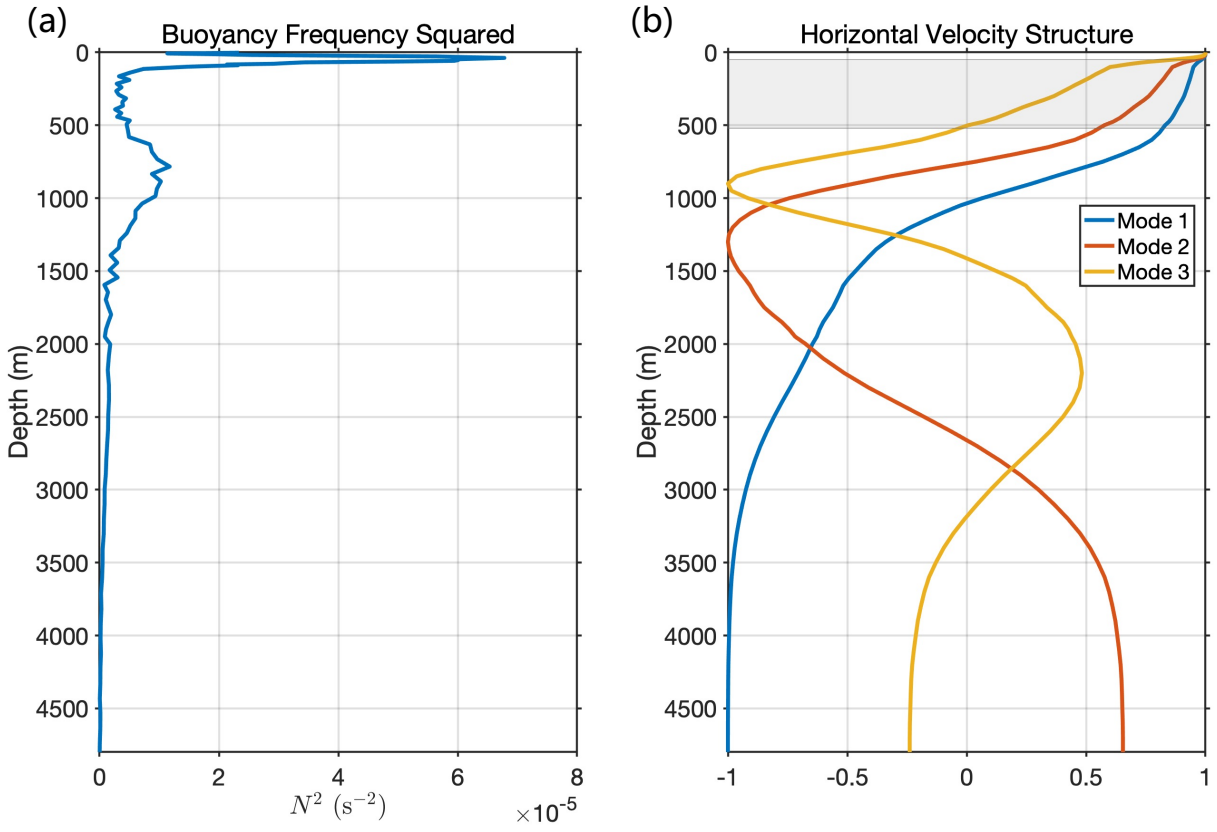


**Figure S6.** (a) Climatological mean stratification $N^2$ computed from WOA18 at the point nearest to the mooring site and (b) the first three modes for horizontal velocity. Grey shading represent the central mooring's vertical sampling range.

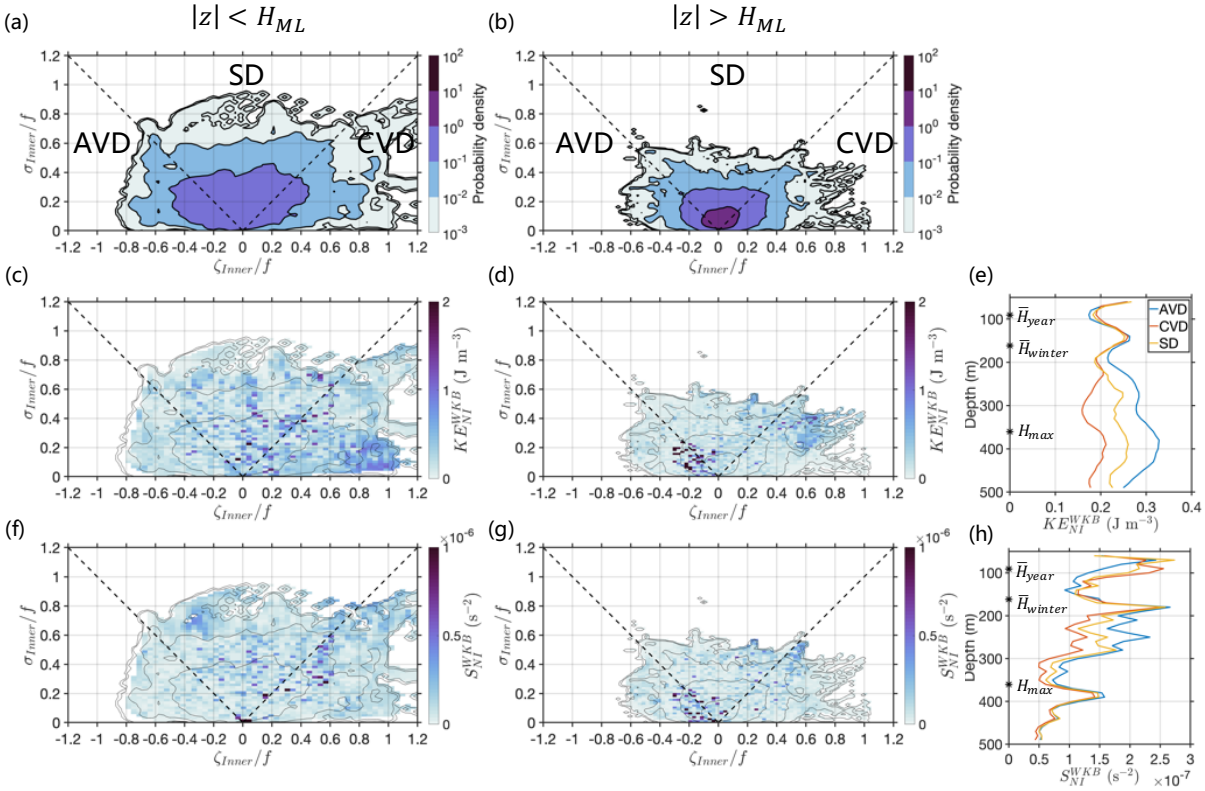


**Figure S7.** Vorticity-strain joint probability density function estimated from the inner moorings (a) within the mixed layer $|z| < H_{ML}$ and (b) below the mixed layer $|z| > H_{ML}$. The x-y space is divided into three regions: anticyclonic vorticity dominated (AVD), cyclonic vorticity dominated (CVD), and strain dominated (SD). Conditional mean of (c-d) $KE_{NI}^{WKB}$ and (f-g) $S_{NI}^{WKB}$ conditioned on the vorticity and strain in the two vertical parts, contoured by the respective probability density. Annual-averaged composite profiles of (e) $KE_{NI}^{WKB}$ and (h) $S_{NI}^{WKB}$ for the AVD, CVD and SD regions. The annual-averaged, winter-averaged and maximum mixed layer depths, respectively denoted by $\overline{H}_{year}$, $\overline{H}_{winter}$ and $H_{max}$, are marked on the y axis of panels (e) and (h).